Check for updates

ADVANCED SUSTAINABLE SYSTEMS
www.advsustainsys.com

Electrochemical Deposition of Manganese Oxide on Paper-Based Laser-Induced Graphene for the Fabrication of Sustainable High-Energy-Density Supercapacitors

Maykel dos Santos Klem, Rodrigo Abreu, Tomás Pinheiro, João Coelho, Neri Alves,* and Rodrigo Martins**

Laser-induced graphene (LIG) is widely used to fabricate microsupercapacitors (MSCs) on various sustainable substrates, such as wood, cork, and lignin. However, the fabrication of MSCs, especially high energy density devices on paper, has rarely been reported. In this work, LIG electrodes are fabricated on wax-coated paper, followed by electrochemical deposition of manganese oxide (MnO_2). The obtained LIG/MnO_2 supercapacitors exhibit a maximum areal capacitance of 86.9 mF cm^{-2}, while a device with pristine LIG electrodes exhibit a capacitance of 9.1 mF cm^{-2}, both measured at a current density of 0.1 mA cm^{-2}. In addition, the supercapacitor exhibits good cycling stability, retaining 80% of its initial capacitance after 1000 charge/discharge cycles at a current density of 1 mA cm^{-2}. Notably, the LIG/MnO_2 supercapacitor exhibits an exceptionally high energy density of 7.3 µWh cm^{-2} at a power density of 38.8 µW cm^{-2}. In summary, a simple, fast, scalable, reproducible, and energy-efficient fabrication method is represented using electrochemical deposition of manganese oxide on paper-based laser-induced graphene, which are natural, abundant, and sustainable materials, paving the way for large-scale production of environmentally friendly supercapacitors.

1. Introduction

Graphene is widely regarded as a remarkable material due to its exceptional mechanical, electrical, and thermal properties. In the field of energy storage, graphene's large surface area and excellent electrical conductivity render it an optimal material for supercapacitor (SC) applications.[1] Among the many methods for synthesizing and depositing graphene laser-induced graphene (LIG) is one of the most studied materials for SC fabrication.[2] LIG is a simple, one-step, low-cost method for producing graphene and designing devices directly on carbon-based substrates. Under laser irradiation,[3] the surface's carbon-hydrogens bonds are cleaved and the sp^3 carbon atoms are converted to sp^2 carbon atoms via a photothermal conversion process.[2] As a result, LIG consists of an electrically conductive porous, interconnected network with a high surface area, which enhances electrochemical performance and charge transport.[2] Additionally, LIG is formed directly on the substrate, simplifying the SC manufacturing process as it can be used as both a current collector and active material.[2–6]Despite the promising figures of merit reported for LIG-SC, with specific capacitances ranging from 50 µF cm^{-2} to 5 mF cm^{-2} and sheet resistances as low as 5 Ω sq^{-1}, carbon-based supercapacitors will always exhibit relatively low energy densities.[7–10] It is therefore not surprising that several strategies have been developed to improve the performance of LIG supercapacitors. LIG doping and decoration with pseudocapacitive materials are the most used approaches. For example, Imbrogno *et al.*, treated a cork substrate with boric acid before the lasing process.[3] The capacitance of the

M. dos S. Klem, N. Alves
São Paulo State University (UNESP)
School of Technology and Sciences
Presidente Prudente, São Paulo 19060-900, Brazil
E-mail: neri.alves@unesp.br

The ORCID identification number(s) for the author(s) of this article can be found under https://doi.org/10.1002/adsu.202400254

© 2024 The Author(s). Advanced Sustainable Systems published by Wiley-VCH GmbH. This is an open access article under the terms of the Creative Commons Attribution License, which permits use, distribution and reproduction in any medium, provided the original work is properly cited.

DOI: 10.1002/adsu.202400254

R. Abreu, T. Pinheiro, J. Coelho, R. Martins
CENIMAT|i3N
Department of Materials Science
School of Science and Technology
NOVA University Lisbon and CEMOP/UNINOVA
Campus de Caparica
Caparica 2829-516, Portugal
E-mail: jmesquita@us.es; rfpm@fct.unl.pt

J. Coelho
Departamento Física de la Materia Condensada
Instituto de Ciencia de Materiales de Sevilla
Universidad de Sevilla—CSIC
Avenida Reina Mercedes SN, Sevilla 41012, Spain

23667486, 2024, 12, Downloaded from https://advanced.onlinelibrary.wiley.com/doi/10.1002/adsu.202400254 by Universidade Estadual Paulista, Wiley Online Library on [05/11/2026]. See the Terms and Conditions (https://onlinelibrary.wiley.com/terms-and-conditions) on Wiley Online Library for rules of use; OA articles are governed by the applicable Creative Commons License

resulting boron-doped LIG supercapacitors increased approximately threefold. Similarly, Parthiban *et al.* showed that doping LIG with both phosphorus and nitrogen resulted in a 16-fold increase in capacitance compared to conventional LIG.[11] More recently, Reina *et al.*, showed that nitrogen doping of LIG together with vacuum-assisted infiltration of an activated carbon slurry resulted in a two-order-of-magnitude improvement in specific capacitance up to 20 mF cm^{-2}.[12] Electrodeposition is another useful method for improving the electrochemical properties of LIG electrodes. It is a very versatile and simple technique that allows the deposition of electrochemically active materials such as metal oxides,[13] polymers,[14] and carbon materials,[14] among others. For instance, Cao *et al.*, electrodeposited polypyrrole onto Kapton-based LIG electrodes. These were then used to assemble asymmetric zinc-ion hybrid microsupercapacitors (MSCs) which exhibit remarkable capacitances (149 mF cm^{-2}).[14] Similar reports can be found for electrodeposited FeOOH and MnO_2 on polyethersulfone (PES),[15] $NiCo_2S_4$,[16] and ZnO[17] on Kapton, As it can be seen, polyimide (Kapton) and other plastic polymers are substrates of choice for LIG-based supercapacitors fabrication.[2] However, cellulose-based substrates, namely wood, cork, and paper, have also attracted scientists' attention because of their environmentally friendly nature and porous structure.[3–6] Due to its volatility at high temperatures and poor mechanical properties when wet, the fabrication and applications of LIG on paper are severely limited. Nevertheless, by impregnating paper substrates with fire-retardant materials it was possible to fabricate carbon-based sensors and MSCs.[4]

In this work, the electrodeposition of manganese oxide on wax coated paper-based LIG electrodes is proposed as a method to fabricate sustainable MSCs with enhanced energy density. Upon lasing, the paper cellulose fibers are converted into a highly porous LIG structure increasing the area available for the deposition of MnO_2. Due to its hydrophobicity, the wax keeps the integrity of the substrate thus allowing for the electrochemical deposition process. By adapting the laser parameters and the deposition times it was possible to produce supercapacitors with a capacitance of 86.9 mF cm^{-2} at 0.1 mA cm^{-2} leading to an energy density as high as 7.3 μWh cm^{-2} at a power density of 38.8 μW cm^{-2}. In this way, we produced sustainable high-energy-density supercapacitors using biodegradable materials. Although the modification of LIG electrodes with MnO_2 has already been reported on other substrates, to the best of the author's knowledge there are still no studies citing the electrodeposition of MnO_2 on LIG converted from paper.

2. Results and Discussion

2.1. Characterization and Optimization of LIG Electrodes

A scheme illustrating the production process of the electrodes and the supercapacitors is shown in **Figure 1a**. First, a layer of wax is printed on both sides of the paper to enhance the substrate's mechanical stability and to create a hydrophobic barrier, thus allowing the electrochemical deposition process. Then, to determine the best parameters for producing LIG on wax-coated paper substrates, an 8 × 8 matrix was constructed by varying the parameters power (P) and raster scan speed (S). The columns represent the percentage power values from 1 to 8% (0.5 to 4 W), while the rows represent the speed with percentage values from 1 to 8% (1.27 to 10.16 cm s^{-1}). The distance from the laser nozzle to the substrate was kept constant at 0.79 mm. The obtained matrix can be seen in Figure 1b. It can be observed that the combination of high power and low speed can cause the complete ablation of the substrate, converting the cellulose into volatile products, even with the fire-retardant treatment. On the other hand, low power and high speed do not seem to provide the necessary energy to convert the substrate into graphitic carbon. Analyzing the matrix, we found that the parameters with the same energy and power percentages produced better films, i.e. the films from the matrix diagonal. Thus, we choose these processing conditions to proceed with the following characterizations.

Figure 1c shows SEM images for the films prepared with power and speed (P:S) ratios varying from 1:1 to 8:8. As can be seen, the fiber structures are preserved when low P:S combinations are used. In addition, volatile products are released during laser irradiation, causing the porosity observed in the carbonized fibers.[18] The porosity of LIG is one of the main characteristics that make this material a good choice for applications in energy storage devices.[19,20] It is also possible to observe in Figure 1c that the fiber structures are partially destroyed for parameters higher than 6:6, suggesting thermal degradation. Thus, films 6:6, 7:7, and 8:8 presented low mechanical stability, being more able to crack during manipulation.

To study the conversion process from paper to LIG, the elemental composition of the films was studied by EDS. Figure 1d shows the atomic percentages obtained from the EDS characterizations for the LIG films (1:1 to 8:8) and for the paper with wax before laser irradiation. The waxed paper showed a higher percentage of oxygen than carbon, which is consistent with the composition of cellulose molecules.[21] The relative percentage of carbon increases for all irradiated samples compared to paper/wax, indicating the release of oxygen during the conversion of the substrate into LIG. The relative percentage of carbon reaches its maximum for the 3:3, 4:4, and 5:5 films, with a percentage of around 80%. In the 6:6, 7:7, and 8:8 samples, there is a tendency for carbon content to decrease while the oxygen content slightly increases. This suggests that less cellulose/paraffin is converted into LIG at these parameters, mainly because the substrate starts to degrade.

Raman spectroscopy was carried out to study the chemical structure of the prepared samples. The spectra obtained are shown in Figure 1e. and all of them show three peaks commonly assigned to graphitic materials.[22,23] These peaks are located at 1320, 1580, and 2650 cm^{-1}, which are assigned to the D, G, and 2D vibrational modes, respectively.[24,25] The D band is generally associated with defects in disordered graphitic structures and is not detectable in pristine graphene and graphite single crystals. The G band is related to the ordered hybridized sp^2 carbon atoms, and the is addressed to second-order phonon.[26] The presence of a 2D peak at 2650 cm^{-1} indicates the formation of graphitic carbon structures composed of a small number of layers.[19,27] The intensity ratio I_D/I_G provides an estimate of the defect density and relative quality of the LIG produced. By taking the intensity of the corresponding D and G peaks, the I_D/I_G ratios varied from 1.44 to 1.17 for the 1:1 and 7:7 films, respectively. The ratio then increases again to 1.38 for the 8:8 film, indicating the formation of defective graphene as the power and speed parameters

 © 2024 The Author(s). Advanced Sustainable Systems published by Wiley-VCH GmbH

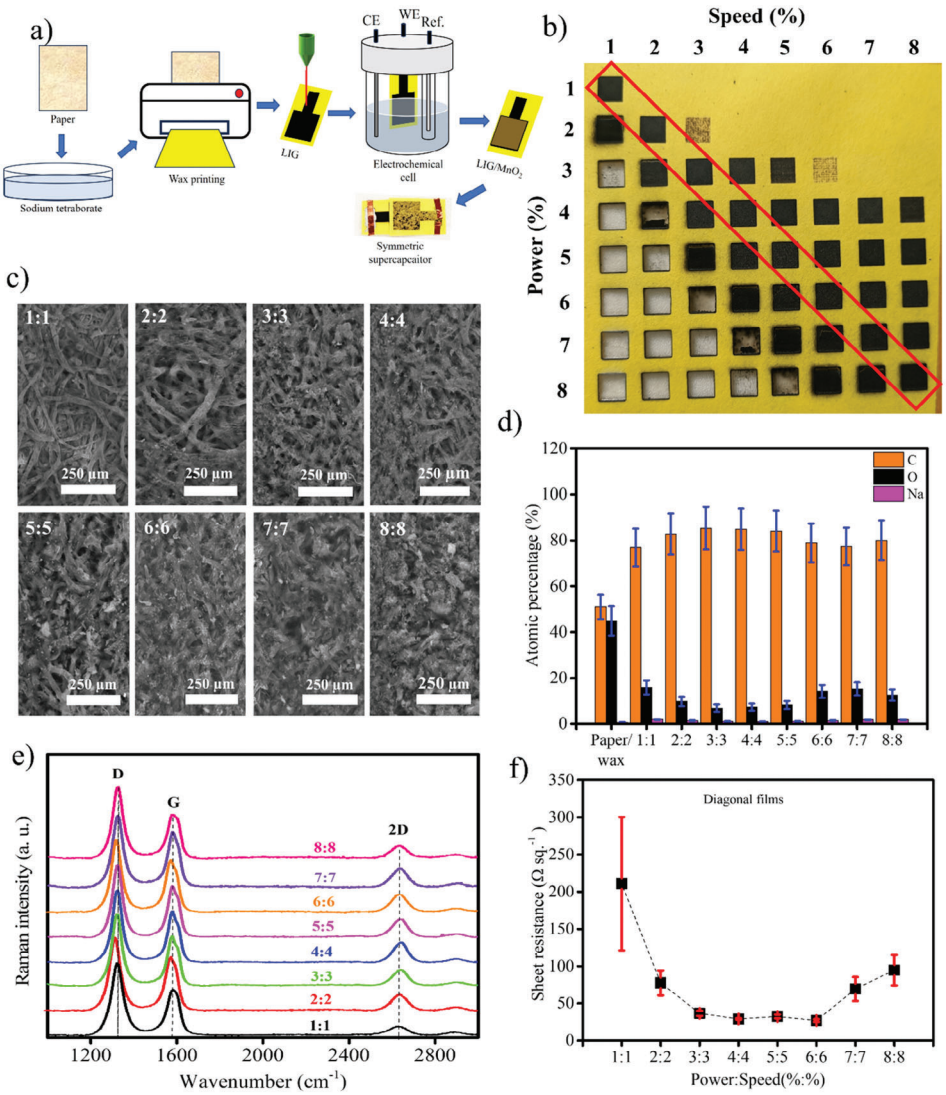


Figure 1. a) Scheme showing the fabrication of LIG on paper and the electrochemical deposition of MnO_2 on LIG. Briefly, a piece of paper Whatman is soaked in sodium tetraborate. After drying, a layer of paraffin wax is printed on it. The substrate is converted into LIG by laser irradiation, and then a layer of MnO_2 is electrodeposited over the as-prepared electrode. Finally, two identical electrodes, separated by a piece of paper soaked in PVA/LiCl, as pressed face-to-face to assembly the supercapacitor. b) 8 × 8 matrix construction with the Power (P) and Speed (S) parameter percentages in the rows and columns respectively. c) SEM images for the films fabricated with the parameters from the matrix diagonal 1:1 to 8:8 (%:%). d) Atomic percentage plot obtained from EDS analysis for the LIG films and paper/wax substrates. e) Raman spectrum for the LIG films obtained using an excitation laser at 1.3 nm. d) Normalized atomic percentage plot obtained from EDS analyses for the LIG films and paper/wax substrates. e) Raman spectrum for the LIG films obtained using a 633 nm excitation laser. f) Sheet resistance values for the LIG films from the matrix diagonal.

increase.[28] However, this improvement reaches a limit of 8:8 when the substrate starts to suffer from thermal degradation, as we observed in the previous characterizations. The ratio I_{2D}/I_G values increased from 0.29 to 0.5 for the 1:1 and 5:5 films, respectively, indicating a reduction in the number of graphene layers.[27] We found I_{2D}/I_G values that increased from 0.29 to 0.5, for the 1:1 and 5:5 films, respectively, suggesting a reduction in the number of graphene layers (Figure S1, Supporting Information). Similar results were found by Pinheiro *et al.*, for LIG films prepared from chromatography and office paper substrates.[29] The quality of the LIG films is also directly related to their electrical properties, as can be seen from the sheet resistance plot in Figure 1f. As expected, the lowest sheet resistances were found for the 3:3, 4:4, 5:5, and 6:6 films, which had better chemical/morphological properties in the previous characterizations. The lowest sheet resistance value was found for the 6:6 film (26.9 ± 1.8 Ω sq^{-1}) followed by the 4:4 (29.0 ± 0.9 Ω sq^{-1}). These values agree with other work found in the literature on LIG fabricated on paper substrates.[30] Recently, Coelho *et al.*, reported the successful fabrication of high-capacity microsupercapacitors using paper-based LIG electrodes with sheet resistances of 30 Ω sq^{-1}.[4]

The direct irradiation of paper led to the production of reasonably good LIG films. However, recent work has reported that successive laser scans can produce graphene with better

© 2024 The Author(s). Advanced Sustainable Systems published by Wiley-VCH GmbH

23667486, 2024, 12, Downloaded from https://advanced.onlinelibrary.wiley.com/doi/10.1002/adsu.202400254 by Universidade Estadual Paulista, Wiley Online Library on [05/11/2026]. See the Terms and Conditions (https://onlinelibrary.wiley.com/terms-and-conditions) on Wiley Online Library for rules of use; OA articles are governed by the applicable Creative Commons License

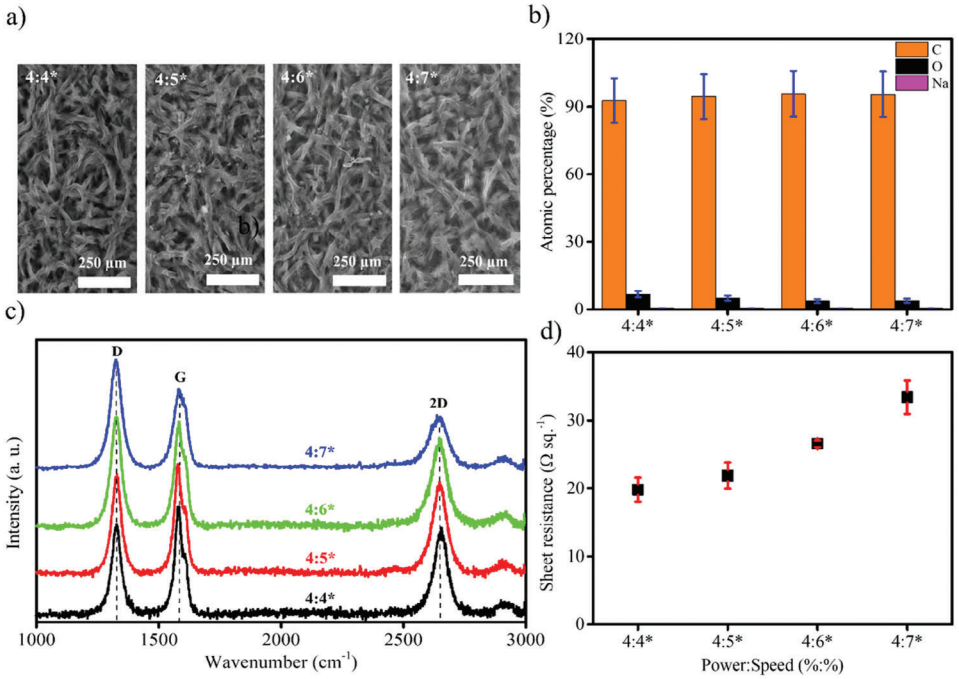


Figure 2. a) Sem images for the LIG films with two laser irradiations with parameters P:S parameters for the second scan varying from 4:4 to 4:7. All films were prepared with a first scan at 4:4 b) Atomic percentage plots obtained from the EDS analyses showing the presence of C, O, and Na. c) Raman spectrum acquired with a 633 nm excitation laser. d) Sheet resistance plots for the 4:4*, 4:5*, 4:6*and 4:7* LIG films.

chemical/structural properties and consequently lower film resistances.[10] Since electrode conductivity is one of the key factors in producing supercapacitors with higher power densities, we investigated the fabrication of LIG with two laser irradiation scans in the same substrate area. As seen before, the 6:6 film had a lower sheet resistance. However, the film obtained is too thin and can crack during manipulation. Therefore, for the first scan, we chose the parameter combination 4:4 (%:%), which was kept the same for all the films tested here. For the second scan, we kept the power at 4% and only varied the speed (S) from 4 to 7%. The LIG films obtained after two laser exposures are marked with an asterisk (*) in this text. The nomenclature is with respect to the second irradiation parameters since all films were produced with a first irradiation of 4:4. As before, the film's morphological characterization was studied again by SEM. The micrographs in **Figure 2** shows that the second irradiation still preserves the structure of the paper fibers. In addition, the fibers appear to be further apart, further increasing the porosity of the films. This may imply higher double-layer capacitances when the films are used as supercapacitor electrodes.[12] Figure 2b shows the relative percentages of C, O, and Na found for the LIG films from EDS measurements. The relative percentage of C was found to be around 90%, a higher value than for the single-exposure films. The increase in the relative percentage of C in LIG films was also observed by Pinheiro *et al.*, after several successive laser scans.[10] This indicates an improvement in the conversion of cellulose and wax into graphene after the second irradiation.

To verify these changes in the LIG obtained with two laser scans, Raman spectroscopy analyses were carried out on the films. The spectrum obtained is shown in Figure 2c. The G peaks are more intense than the D peaks for the 4:4* and 4:5* films, indicating graphene with fewer defects. The 4:5* films presented an I_D/I_G ratio of 0.9, a lower value than that found with only one laser irradiation. Furthermore, this I_D/I_G ratio is lower than others found for LIG films made from paper and cotton cloth.[31] In addition, the $I_{2D}/I_G > 1$ for all films indicates the production of few-layer graphene sheets, proving the quality improvement caused by the second laser scan (Figure S1b, Supporting information). The quality improvement can also be observed in the sheet resistance plot shown in Figure 2d. The 4:4* sample exhibited a sheet resistance of 19.8 ± 1.8 Ω sq^{-1} followed by the 4:5* with 21.9 ± 1.9 Ω sq^{-1}. Reina *et al.*, reported LIG electrodes fabricated from polymeric substrates for supercapacitor applications with a sheet resistance of 30 Ω sq^{-1}.[12] However, as the 4:4* film presented poor mechanical properties toward handling, the 4:5* conditions were chosen to fabricate the supercapacitor electrodes.

2.2. Deposition and Characterizations of MnO_2/LIG Films

Manganese oxide was electrodeposited on LIG electrodes (4:5*) using manganese acetate as a precursor in a conventional electrochemical cell. The LIG electrodes were subjected to a constant potential of 0.9 V (vs Ag/AgCl). In addition, electrodes were prepared with three different deposition times to evaluate the synthesis/deposition process: 1-, 3-, and 5 min. A mechanical failure of the electrodes was observed above a deposition time of 5 min. This was due to the electrodes cracking, peeling off, or detaching completely from the paper substrate. As a result, the deposition time was limited to a maximum of 5 min. MnO_2 was chosen, as it is a well-established material with a known electrochemical

© 2024 The Author(s). Advanced Sustainable Systems published by Wiley-VCH GmbH

23667486, 2024, 12, Downloaded from https://advanced.onlinelibrary.wiley.com/doi/10.1002/adsu.202400254 by Universidade Estadual Paulista, Wiley Online Library on [05/11/2026]. See the Terms and Conditions (https://onlinelibrary.wiley.com/terms-and-conditions) on Wiley Online Library for rules of use; OA articles are governed by the applicable Creative Commons License

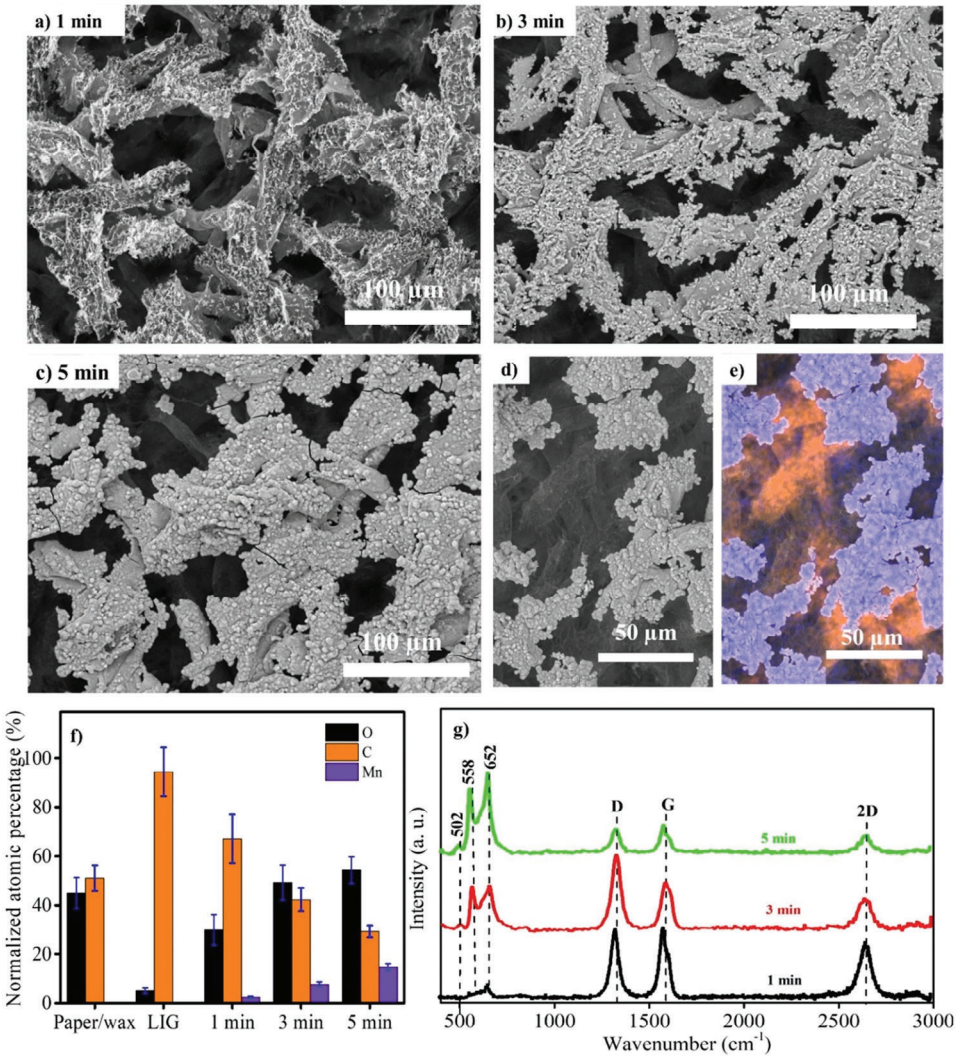


Figure 3. SEM images for the MnO_2 films electrodeposited on LIG different deposition times a) 1 min, b) 3 min, and c) 5 min. d) SEM image showing the region where we performed the e) EDS mapping highlighting the elements Carbon (orange) and Manganese (purple) f) normalized atomic percentage plots obtained from the EDS analyses for the LIG/MnO_2 electrodes revealing the presence of C, O, and Mn. g) Raman spectra for the LIG/MnO_2 electrodes with different deposition times. The measurements were performed with a 633 nm excitation laser.

performance and as such allows to validate our approach.[32,33] **Figure** 3a–c shows SEM micrographs of the LIG/MnO_x electrodes for the different processing times. For the electrode with 1 min deposition time, the LIG fibers appear to be partially covered by the deposited material. For the electrode with 3 min deposition, a considerable amount of material can be seen covering the carbonized fibers. Moreover, the deposited material appears to form micro-sized crystals that agglomerate over the LIG fibers. As seen in Figure 3c, for the deposition time of 5 min there is an increase in crystal size and the deposited material covers a larger surface area. It can also be observed that the material is deposited mainly over superficial fibers. This effect may be related to the inherent hydrophobicity of the LIG films produced in an inert atmosphere.[34] The associated low surface tension appears to prevent electrolyte access to the inner fibers, as it is responsible for the capillary pressure that allows electrolyte infiltration.[35–37] Another supposition is that the LIG's outer surface is more conductive than its bulk, favoring the formation of MnO_2 on the external fibers. Furthermore, this phenomenon could also be related to an electrostatic shielding that prevents ions from accessing the electrode's bulk. We are still not sure about the phenomena of electrodeposition on LIG and more studies are necessary in this regard.

The EDS mapping in Figure 3d,e indicates that the material deposited on the LIG surface is mainly composed of manganese, as expected. It is also possible to see the internal LIG fibers highlighted in orange. The atomic percentages from the EDS analyses and their respective values are plotted in Figure 3f. As expected, the atomic percentages of Mn and O increase with deposition time, while C decreases. To analyze the chemical nature of the electrodeposited material on LIG, the electrodes were subjected to Raman spectroscopy characterization. The spectra obtained are shown in Figure 3g. It is possible to identify the three characteristic peaks D, G, and 2D for the laser-induced graphene, as

© 2024 The Author(s). Advanced Sustainable Systems published by Wiley-VCH GmbH

23667486, 2024, 12, Downloaded from https://advanced.onlinelibrary.wiley.com/doi/10.1002/adsu.202400254 by Universidade Estadual Paulista, Wiley Online Library on [05/11/2026]. See the Terms and Conditions (https://onlinelibrary.wiley.com/terms-and-conditions) on Wiley Online Library for rules of use; OA articles are governed by the applicable Creative Commons License

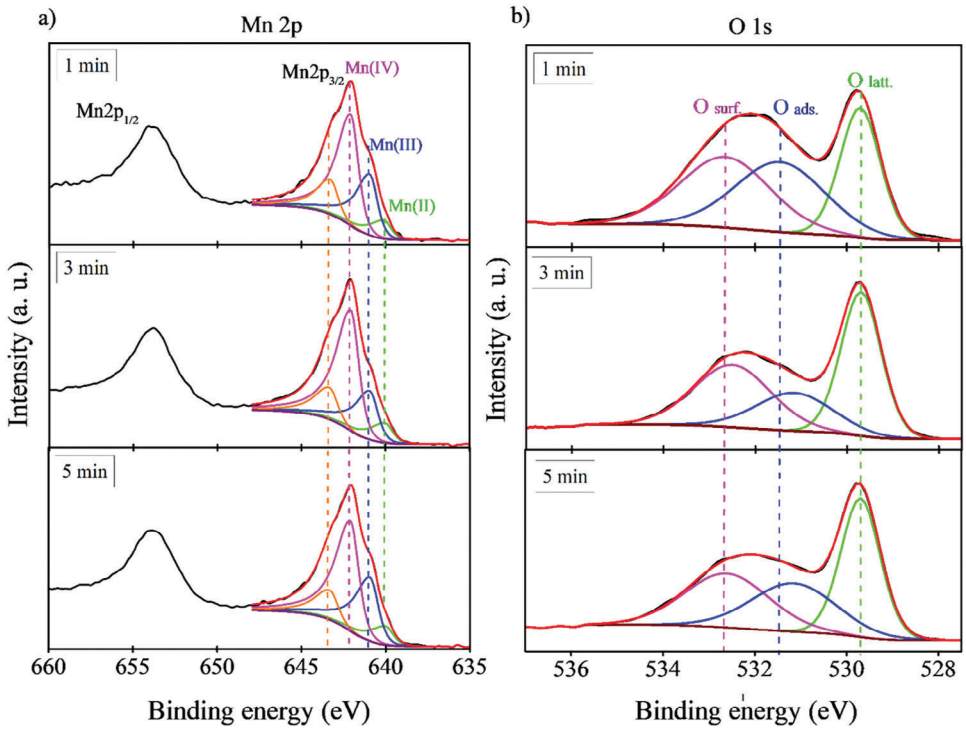


Figure 4. High-resolution XPS spectra of the a) Mn 2p and b) O 1s regions for the LIG/MnO_2 electrodeposited electrodes with different deposition times.

discussed earlier. The Raman spectra also presented peaks located at 502, 558, and 652 cm^{-1} that are associated with the manganese dioxide (MnO_2) vibrational modes.[38–40] The 650 cm^{-1} band can be attributed to the stretching vibrations of Mn—O bonds, while the 560 cm^{-1} band is attributed to the stretching of Mn—O in the basal plane of MnO_6.[39] There are discussions in the literature about the assignment of the peak at 650 cm^{-1} to the manganese oxide in the stoichiometric form Mn_3O_4.[41] Bernard *et al.* discussed the difficulty of assigning a Raman spectrum to the MnO_2, since Mn^{4+} cations are thermodynamically unstable and easily reduced.[42] It is also known that Mn_3O_4 can be obtained from the thermal decomposition of MnO_2.[43] Thus, as discussed in the literature, the presence of Mn_3O_4 can be attributed to the local heat caused by the Raman excitation laser.[26,27] The peaks become more intense as the deposition time increases, indicating a greater amount of material being deposited/synthesized on the LIG electrode. Further structural analysis was conducted by XRD, however no significant results were obtained from the measurement (Figure S2, Supporting Information). It should be noted that electrodeposited MnO_2 generally forms layered structures with turbostratic disorder in the (00l) planes and variable interlayer spacing (the prime example being birnessite type δ-MnO_2 that stabilizes with Na^+ ions). When layered MnO_2 is deposited on flat substrates, these layers lie parallel to the substrate and, since in the Bragg-Brentano geometry in XRD the scattering vector lies perpendicular to the sample, most of the scattering is due to the (00l) planes which do not have a well-defined spacing. Thus, it is sometimes difficult to obtain well-defined Bragg peaks from layered MnO_2.[44] This behavior is also observed for MnO_2 electrodeposited on carbon nanotubes,[45] stainless steel,[46] and reduced graphene oxide,[47] where the XRD diffractograms do not indicate (or barely) the presence of manganese oxide.

To validate the findings from the Raman spectroscopy analysis, we conducted XPS measurements on the electrodeposited electrodes. **Figure 4a** displays the Mn2p fine spectra for films electrodeposited for 1, 3, and 5 min. The spectra consist of Mn $2p_{1/2}$ and Mn $2p_{3/2}$ peaks with a spin-orbit splitting of 11.8 eV, a value commonly documented in the literature for manganese oxides.[48] To assess the Mn oxidation state, we performed deconvolution of the Mn $2p_{3/2}$ peaks. The deconvolution process revealed four additional peaks, demonstrating the expected multiplet splitting for manganese oxides.[49] The peak at a binding energy of 640.0 eV corresponds to manganese in the Mn(II) oxidation state, while the peak at 640.9 eV is attributed to Mn(III). The peak at 642.1 eV can be associated with the Mn(IV) oxidation state and is accompanied by a satellite peak at 643.3 eV.[50,51] The presence of different manganese oxidation states in MnO_2 samples has been reported in the literature by other researchers.[48,49,52] Manganese's inherent tendency for spontaneous oxidation can result in various bonds with oxygen, giving rise to a family of manganese oxides with diverse stoichiometries.[53] Thus, the XPS analyses corroborate the findings of the Raman analysis, indicating the presence of different manganese oxides in the electrodeposited electrodes. Figure 4b shows the O1s spectra obtained for the samples. These spectra can be deconvoluted into three peaks related to: lattice oxygen (Mn—O, $O_{latt.}$) at a binding energy of 529 eV; adsorbed oxygen molecules ($O_{ads.}$) due to oxygen vacancies at a binding energy of 531 eV; and absorbed water on the surface ($O_{surf.}$).[40,54,55] The peak position does not change

© 2024 The Author(s). Advanced Sustainable Systems published by Wiley-VCH GmbH

23667486, 2024, 12, Downloaded from https://advanced.onlinelibrary.wiley.com/doi/10.1002/adsu.202400254 by Universidade Estadual Paulista, Wiley Online Library on [05/11/2026]. See the Terms and Conditions (https://onlinelibrary.wiley.com/terms-and-conditions) on Wiley Online Library for rules of use; OA articles are governed by the applicable Creative Commons License

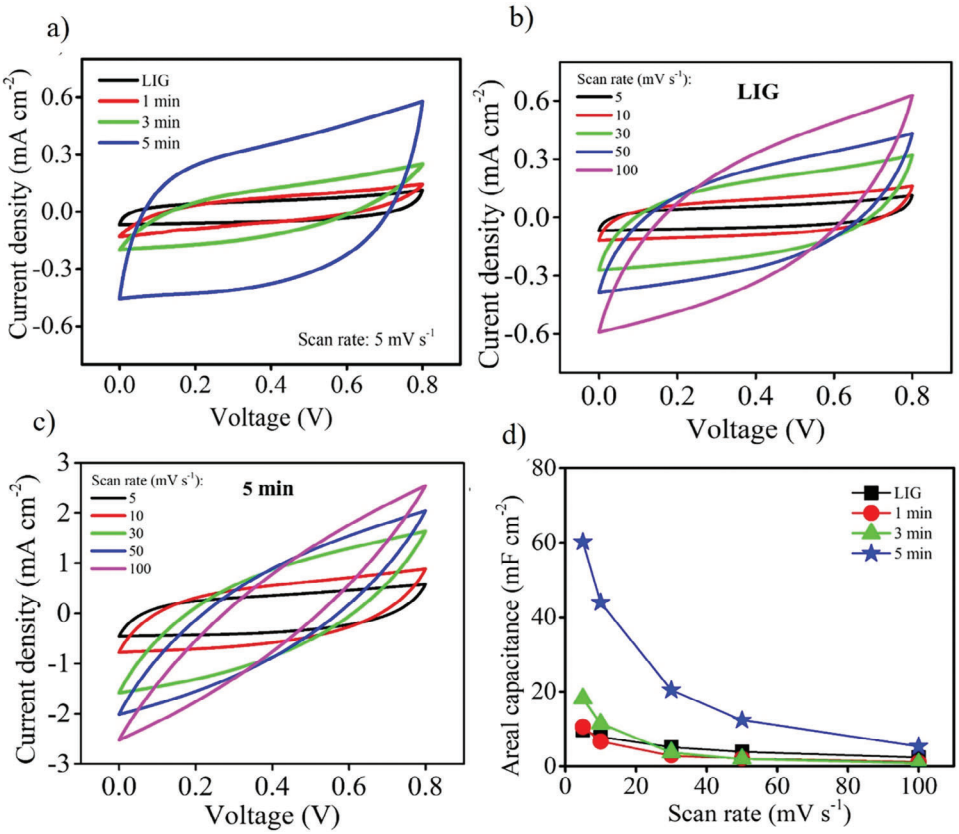


Figure 5. a) Cyclic voltammetry curves for the 1, 3, 5 min, and LIG supercapacitors taken at a scan rate of 5 mV s^{-1}. b), c) Voltammograms for the 5 min and LIG devices obtained at scan rates ranging from 5 to 100 mV s^{-1}.d) Plot of the areal capacitance (C_A) as a function of the scan rate. The capacitances were obtained from the CV curves.

from one sample to another and only a small variation on the O surf. and O ads. quantities can be observed, suggesting that the same manganese phase is being deposited independently of the deposition time.

2.3. MnO_2/LIG on Paper Supercapacitor Assembly and Testing

Symmetrical sandwich supercapacitors were fabricated based on bare LIG on paper and LIG/MnO_2 electrodes with different deposition times, as illustrated in Figure 1a. For the sake of simplicity, supercapacitors were labeled based on their electrode composition: LIG, 1, 3, and 5 min. **Figure** 5a shows the cyclic voltammetry (CV) curves recorded at a scan rate of 5 mVs^{-1}. It can be observed that all devices with electrodes containing MnO_2 showed higher currents than the bare LIG-based supercapacitor. This may indicate an improvement in the capacitive properties of these electrodes due to the pseudocapacitive properties of MnO_2. In addition, the larger area delimited by the CV curves for these devices indicates a greater capacity to store charge.[56–58] For a better comparison, Figure 5b,c shows the voltammetry curves for the 5 min supercapacitor with scan rates ranging from 1 to 100 mV s^{-1}. As can be seen, the device presented capacitive behavior for scan rates lower than 30 mV s^{-1}, evidenced by the curves with rectangular profiles. However, the CV curves showed a major deviation from ideality at scan rates greater than 30 mV s^{-1}, indicating resistive behavior.[35] In comparison, the CV curves for the supercapacitor with LIG-based electrodes maintained a rectangular shape for measurements with high scan rates. As described in the literature, this effect may be related to the high resistivity of MnO_2.[38] In addition, the charge/discharge processes in pseudocapacitive materials are relatively slower than the charge/discharge of an electric double layer in carbonaceous materials,[39,40] The CV curves for the 1 and 3 min devices can be seen in the Figure S3 (Supporting Information).

The areal capacitance (C_A) of the prepared supercapacitors as a function of the applied scan rate is plotted in Figure 5b. The devices exhibited areal capacitances of 60.2, 18.2, 10.5, and 9,7 mF cm^{-2} for the 5, 3, and 1 min e LIG supercapacitors, respectively, at 5 mV s^{-1}. The effect of MnO_2 electrochemical activity becomes clearer with longer deposition times, as the 5 min device exhibited a capacitance nine times higher than that obtained for the supercapacitor with bare LIG electrodes We can also see that the capacitance values tend to decrease as the scan rate increases. This happens because fewer ions have time to reach the inner electrode´s surfaces at faster scans. Moreover, fast measurements also reduce the time that ionic species must interact with the interfaces, disfavoring slow storage processes such as ionic intercalation and redox reactions.[36]

Galvanostatic charge/discharge (GCD) experiments further confirm the CV results. **Figure** 6a shows the GCD curves

© 2024 The Author(s). Advanced Sustainable Systems published by Wiley-VCH GmbH

23667486, 2024, 12, Downloaded from https://advanced.onlinelibrary.wiley.com/doi/10.1002/adsu.202400254 by Universidade Estadual Paulista, Wiley Online Library on [05/11/2026]. See the Terms and Conditions (https://onlinelibrary.wiley.com/terms-and-conditions) on Wiley Online Library for rules of use; OA articles are governed by the applicable Creative Commons License

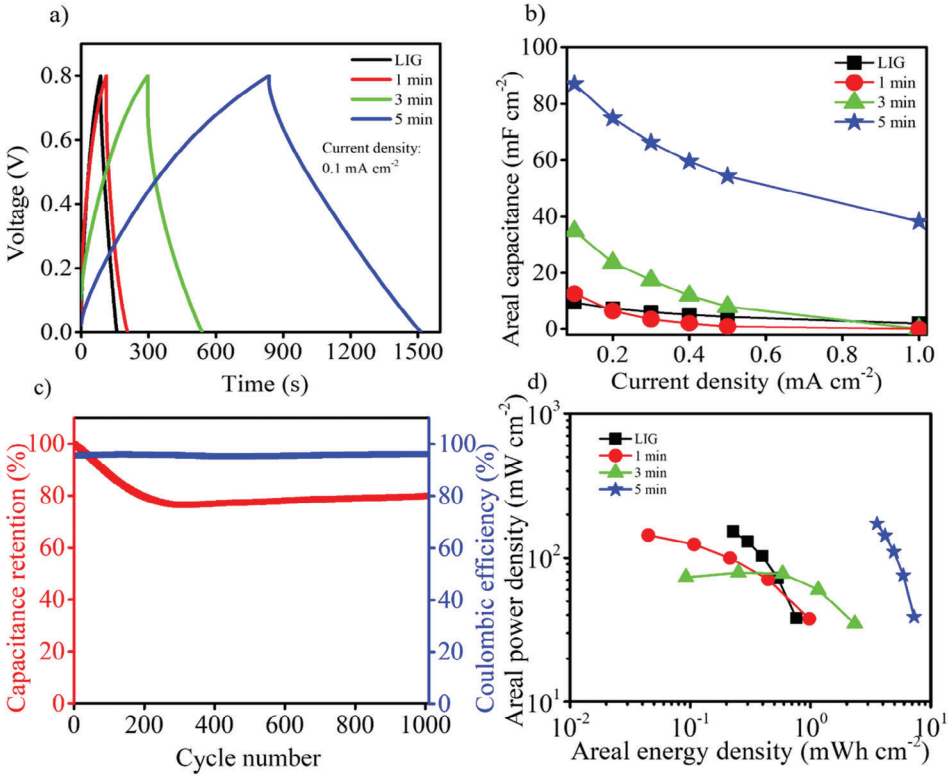


Figure 6. a) Galvanostatic charge/discharge curves for the 1, 3, 5 min, and LIG supercapacitors obtained at a current density of 0.1 mA cm^{-2}. b) Specific capacitance vs. current density varying from 0.1 to 1 mA cm^{-2}. c) Cyclability test and coulombic efficiency for the 5 min supercapacitor showing the specific capacitance as a function of the number of charge/discharge cycles. The cycles were performed at a current density of 0.5 mA cm^{-2}. d) Ragone plot for the LIG, 1, 3, and 5 min supercapacitors.

obtained at a current density of 0.1 mA cm^{-2}. The curves exhibited a near-ideal triangular profile, indicating a capacitive behavior and good storage efficiency. Small deviations from ideality can be attributed to the pseudocapacitive effects of the MnO_2 and electrical resistance of LIG.[59] The GCD curves obtained for the LIG, 1, 3, and 5 min devices varying the charge/discharge current density be seen in Figure S4 (Supporting Information). As can be seen in Figure 6b, the supercapacitors exhibited maximum specific capacitances of 86.9, 34.8, 12.6, and 9.5 mF cm^{-2} for the 5, 3, 1 min, and LIG supercapacitors, respectively, at a current density of 0.1 mA cm^{-2}. The capacitance for the 5 min device is about 9 times higher than for the LIG supercapacitor, in good agreement with the CV analyses. The addition of pseudocapacitive materials to LIG results in a supercapacitor metrics enhancement. Zhu *et al*. reported a supercapacitor with LIG-based electrodes decorated with MnO_2 using PEEK as a substrate. The device exhibited a maximum capacitance of 48.9 mF cm^{-2} at 10 mV s^{-1}.[60] Recently, the same group described the production of supercapacitors with LIG electrodes obtained again from PEEK substrates but now impregnated with three different metal oxides: titanium dioxide (TiO_2), nickel oxide (NiO), and tin dioxide (SnO_2). The device with the best performance was the LIG/SnO_2 electrodes, showing a maximum capacitance of 18.58 mF cm^{-2} at 10 mV s^{-1}.[61] In other work, asymmetric microsupercapacitors were produced with one electrode based on LIG/MnO_2 and the other based on LIG/FeOOH (LIG/MnO_2//LIG/FeOOH). In their study, the LIG was produced through the laser irradiation of polyimide, while the MnO_2 and FeOOH were electrodeposited on the LIG. The authors reported that the device exhibited a maximum specific capacitance of 21.9 mF cm^{-2} for a current density of 0.25 mA cm^{-2}, representing only 25% of the total capacitance we can reach with our paper supercapacitor.[62] Following the niche of biodegradable devices, Lu *et al*., recently reported supercapacitors with LIG electrodes produced through the photothermal conversion of cotton fabric. The cotton substrate was previously treated with a precursor of MnO_x to synthesize the metal oxide during laser irradiation. The supercapacitors exhibited a maximum capacitance of 54.97 mF cm^{-2} at a current density of 0.05 mA cm^{-2}.[63] It is important to stress the fact that LIG-based supercapacitors obtained from natural renewable sources, such as paper, exhibited capacitance values comparable to other LIG-based supercapacitors converted from polyimide.[64,65] It is possible that the treatment with sodium tetraborate may also enhance the overall capacitance of the devices, However, this is an effect that should be present on all samples and it alone cannot explain the high specific capacitance for the 5 min device.

Figure 6c shows the cyclic stability test and the coulombic efficiency plots for the 5 min supercapacitor, both analyses performed at a current density of 0.5 mA cm^{-2}. As can be seen, the capacitance drops from 60 to 47.9 mF cm^{-2} after 1000 charge/discharge cycles, representing a retention of 80% from the initial capacitance. Low cyclability is a commonly known

© 2024 The Author(s). Advanced Sustainable Systems published by Wiley-VCH GmbH

23667486, 2024, 12, Downloaded from https://advanced.onlinelibrary.wiley.com/doi/10.1002/adsu.202400254 by Universidade Estadual Paulista, Wiley Online Library on [05/11/2026]. See the Terms and Conditions (https://onlinelibrary.wiley.com/terms-and-conditions) on Wiley Online Library for rules of use; OA articles are governed by the applicable Creative Commons License

Table 1. Comparison of the main parameters of LIG-based supercapacitors reported in the literature.

Electrode	Substrate	Electrolyte	Capacitance [mF cm^{-2}]	Max. energy density [μWh cm^{-2}]	Max. power density [μW cm^{-2}]	Reference
LIG	Kapton	PVA/H_2SO_4	22.2 (0.05 mA cm^{-2})	3.07	6	[2]
LIG	Poly(p-phenylene-benzobisoxazole) paper	PVA/H_2SO_4	46.3 (0.4 mA cm^{-2})	5.93	–	[75]
LIFG (laser induced foam graphene)	Aramide paper	PVA/H_2SO_4	23.8 (0.2 mA cm^{-2})	2.64	400	[76]
LIG/MnO_2	Polyether ether ketone (PEEK)	PVA/H_2SO_4	48.9 (10 mV s^{-1})	3.1	2.5×10^3	[60]
LIG/MnOx	Cotton cloth		54.97 (0.05 mA cm^{-2})	7.63	78.93	[69]
LIG/MnO_2	Paper with wax	PVA/LiCl	60.2 (5 mV s^{-1}) 86.9 (0.1 mA cm^{-2})	7.3	172.2	This work

problem for pseudocapacitive materials, caused by irreversible reactions that degrade the electrodes.[66] Particularly, MnO_2 is known for the low cyclability caused by the dissolution of the material into the electrolyte during the cycling processes.[67] Even so, we can also find studies reporting supercapacitors with electrodes based on LIG,[68] LIG/AgNW,[69] and LIG/SnO_2[69] that also exhibit capacitance retention of 80%. It is also important to note that the major capacitance drop happens during the first 250 charge/discharge cycles. Afterwards, the capacitance starts to increase again reaching a final value of 47.9 mF cm^{-2} after the 1000th cycle. The 5 min supercapacitor also exhibited a high and constant coulombic efficiency of 96% during the 1000 cycles. This value is close to that presented for a supercapacitor with LIG electrodes obtained from polyimide substrates.[70]

The energy and power densities are the main parameters used to evaluate the performance of energy storage devices. Figure 6d shows the Ragone plot for the LIG, 1, 3, and 5 min symmetric supercapacitors. As can be seen, all devices exhibited high values of energy and power density. The 5 min supercapacitor exhibited an outstanding energy density of 7.3 μWh cm^{-2} for a power density of 38.9 μW cm^{-2}; and a high-power density of 172.2 μW cm^{-2} for an energy density of 3.6 μWh cm^{-2}. The energy density reported here is at least two times higher than the values found in the literature for supercapacitors based on LIG produced from non-biodegradable polymers, such as polyimide.[2,71,72] In the biodegradable device's scenario, Coelho *et al.*, reported the production of a supercapacitor with LIG electrodes on paper, which exhibited an energy density of 0.3 μWh cm^{-2}.[4] The supercapacitor with LIG/MnO_x electrodes produced from cotton fabric, mentioned before, presented an energy density close to that obtained here for the 5 min supercapacitor (7.63 μWh cm^{-2}). This demonstrates the synergistic effect between manganese oxides and LIG. However, the power density of this supercapacitor based on LIG from cotton is relatively lower than that exhibited for the 5 min supercapacitor (172.2 μW cm^{-2}). For comparative purposes, **Table 1** summarizes some previously described results, demonstrating the specific capacitance, energy, and power density values for some LIG-based supercapacitors reported in the literature. The produced samples exhibit higher capacitances when compared to pure LIG, due to the pseudocapacitive contribution of MnO_2.[60,73] A relatively high specific capacitance was also measured, probably due to the high areal surface of the substrate.[73] However, these devices were prepared by a rather complex procedure. It is also common to deposit a layer of the metal oxide precursor on the substrate before the lasing process.[60] Specific capacitances of 48.9 mV s^{-1} were measured for polyether ether ketone substrates covered with a film of manganese acetate tetrahydrate.[60] Nevertheless, in this instance, not all the precursor has been utilized, and the impact of the unreacted material has yet to be determined. Nevertheless, this approach could be of interest for porous substrates such as paper. As the precursor's solution is absorbed on the substrate structure, it is possible to obtain 3D electrodes with enhanced capacitance.[4,74]

It can be posited that the electrodeposition of MnO_2 on LIG represents a promising avenue for the development of high-performance and energy-dense LIG on paper supercapacitors. The ability to control the amount of oxide deposited and the deposition of the oxide solely on the electrodes represents a significant advantage, as it maximizes the utilization of the active material. To the author's knowledge, no evidence paper-based LIG electrodes with electrodeposited MnO_2 have been reported.

In order to gain a deeper insight into the charge storage process on the prepared samples, electrochemical impedance spectroscopy (EIS) analyses were also conducted on the 1, 3, 5 min, and LIG supercapacitors. The results are shown in **Figure 7a**.

The spectra showed significant differences between the devices based on LIG/MnO_2 and the ones based only on LIG. The spectrum for the LIG supercapacitor presents the typical shape expected for electric double-layer capacitors (EDLC). On the other hand, the spectra for supercapacitors containing MnO_2 reach lower heights on the imaginary impedance axis (-Z''), indicating higher capacitances.[43] Additionally, low inclinations at low frequency are indicative of charge storage processes involving ionic diffusion and redox reactions.

A scheme of the supercapacitor equivalent circuits is shown in Figure 7b. The fitting parameters can be consulted in the Supporting Information. The phenomena occurring at higher frequencies are represented by the equivalent inductance L in series with an equivalent resistance R_s, both in series with a modified Randle's circuit. The equivalent inductance L only appears for devices with electrodes containing MnO_2. Its occurrence in electrochemical systems is not very well understood, but some authors attribute the appearance of this effect to the measurement system.[77] As can be seen in Table S1 (Supporting Information) from supplemental information, the equivalent series resistance R_s values vary from 132.9 Ω, for the LIG

© 2024 The Author(s). Advanced Sustainable Systems published by Wiley-VCH GmbH

23667486, 2024, 12, Downloaded from https://advanced.onlinelibrary.wiley.com/doi/10.1002/adsu.202400254 by Universidade Estadual Paulista, Wiley Online Library on [05/11/2026]. See the Terms and Conditions (https://onlinelibrary.wiley.com/terms-and-conditions) on Wiley Online Library for rules of use; OA articles are governed by the applicable Creative Commons License

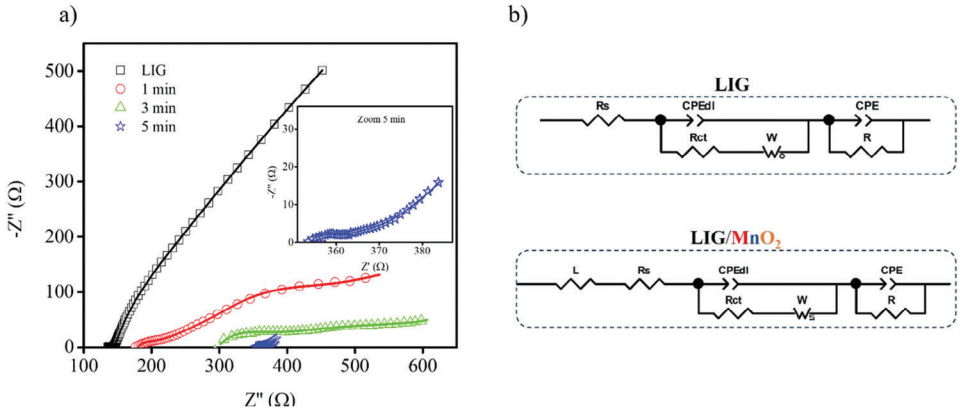


Figure 7. a) Impedance spectra for the LIG, 1, 3, and 5 min supercapacitors. The hollow symbols represent the experimental data while the solid lines are the theoretical values obtained by the fitting using equivalent circuits. In the inset is presented the spectrum for the 5 min device. b) Scheme of the equivalent circuits used to fit the impedance spectra. All the fittings exhibited a low chi-squared of 10^{-4}.

supercapacitor, to a maximum of 346.1 Ω, for the 5 min device. This effect was expected since MnO_2 is a semiconductor that has low conductivity.[78] In the branch of the modified Randle's circuit, CPEdl represents the interfacial phenomena related to the formation of the electric double layer. As shown in Table S1 (Supporting Information), this parameter tends to decrease as the amount of MnO_2 increases. It is expected that the capacitance of devices based on LIG/MnO_2 presents lower values at high frequencies due to the slower storage mechanisms of the MnO_2. This is the same effect seen in the CV and GCD curves for high scan rates and high current densities, respectively. However, it may suggest a reduction as well on the available electrochemical surface area. In Randle's circuit, we also have the R_{ct} parameter that represents the resistance of charge transfer between the electrodes and the electrolyte. We can see in Table S1 (Supporting Information) that most Rct values tend to increase with the amount of MnO_2 deposited on LIG.

The last parameter found in the Randle circuit is related to the finite Warburg diffusion, which can be described by two different circuit elements: the open circuit (Wo) and the short circuit (Ws). The Wo arises when diffusive species encounter a reflexive boundary, such as carbonaceous material. On the other hand, when the diffusive species reaches an electroactive boundary, the impedance spectra will be better represented by Ws. Therefore, the diffusion phenomena in the impedance spectra are represented by Wo in the LIG supercapacitor, while the diffusion found for supercapacitors with MnO_2 is better fitted using Ws.

The last branch of the equivalent circuit is given by a parallel R-CPE circuit that represents the phenomena occurring at low frequencies. This branch may be related to a pseudocapacitive effect when electroactive electrodes are used. At the same time, it may also be associated with side reactions that occur when electric fields are applied to the electrodes over a long period. As can be seen in Table S1 (Supporting Information), Q values tend to increase with the amount of MnO_2. However, the value of the n parameter decreases, demonstrating that the electrodes tend to resistive behavior. These same characteristics were also found in the CV and GCD analyses, where MnO_2/LIG electrodes exhibited higher capacitances for slower measurements.

3. Conclusion

In this study, we successfully produced high-energy-density supercapacitors through a sustainable approach, using environmentally friendly materials and techniques. Superior LIG films on paper were achieved after subjecting the substrate to two laser irradiation steps. Scanning electron microscopy (SEM) images reveal that these films are highly porous while retaining the inherent structure of the paper fibers. These films demonstrated sheet resistances as low as 21.9 ± 1.9 Ω sq^{-1}. Furthermore, these films were subjected to further functionalization through electrodeposition of MnO_2 on their surface. Through Raman analyses, it was determined that a deposition time of 5 min produced MnO_2 films with enhanced chemical characteristics. SEM images demonstrate that the metal oxide only grew on the surface of LIG, likely due to its hydrophobic properties. When utilized as supercapacitor electrodes, LIG/MnO_2 films with a deposition time of 5 min exhibited the most favorable performance in terms of energy storage. In cyclic voltammetry analyses, these devices demonstrated a specific capacitance per area of 60.2 mF cm^{-2}, which is approximately nine times higher than the value found for the LIG-based devices. This same distinction was observed in the galvanostatic charge/discharge measurements. The 5 min supercapacitor exhibited a significant specific capacitance of 86.9 mF cm^{-2}, measured at a current density of 0.1 mA cm^{-2}. Additionally, the supercapacitor displayed favorable cyclability, retaining 80% of its initial capacitance after 1000 charge/discharge cycles at a current density of 1 mA cm^{-2}. Finally, when compared with other similar devices reported in the literature, LIG/MnO_2 supercapacitors exhibited an exceptionally high energy density of 7.3 μWh cm^{-2} at a power of 172.2 μW cm^{-2}. In summary, laser-induced graphene presents a quick, adaptable, and economical method for creating graphene directly on sustainable substrates. LIG's distinctive characteristics and design flexibility offer significant potential for a wide range of applications, including energy storage, electronics,

© 2024 The Author(s). Advanced Sustainable Systems published by Wiley-VCH GmbH

23667486, 2024, 12, Downloaded from https://advanced.onlinelibrary.wiley.com/doi/10.1002/adsu.202400254 by Universidade Estadual Paulista, Wiley Online Library on [05/11/2026]. See the Terms and Conditions (https://onlinelibrary.wiley.com/terms-and-conditions) on Wiley Online Library for rules of use; OA articles are governed by the applicable Creative Commons License

environmental technology, and sensing. In this study, we report for the first time the functionalization of LIG electrodes made from paper substrates using MnO_2. The study demonstrated the potential use of these electrodes in environmentally friendly, degradable, and pliant high-energy supercapacitors.

4. Experimental Section

Paper Treatment and LIG Electrode Fabrication: First, Whatman paper (grade 1) was soaked in a fire-retardant solution of sodium tetraborate decahydrate (0.1 M) for 30 min and then left to dry overnight in room conditions. A layer of paraffin wax was then printed on the obtained paper using a Xerox ColorQube printer. The waxed paper was placed on a hot plate at 110 °C to melt the wax into the paper. After the fire retardant and wax treatment, the paper substrates were mounted on a glass substrate to keep their surface as flat as possible. The LIG electrodes were then fabricated using a CO_2 universal laser system with an infrared wavelength of 10.6 µm. In this work, LIG was fabricated on paper using 4% of the maximum power and scan speed of both systems, and the distance from the substrate to the laser beam exit was kept at 0.79 mm. This laser system has a maximum power of 50 W and a maximum scan speed of 127 mm s^{-1}. The paper substrates were irradiated twice with the above configurations to improve carbonization and thus the conductivity of the films. Silver ink and conductive copper tape were used as contacts for electrical measurements. All chemicals were used as purchased without further modification.

Electrochemical Deposition of MnO_2: MnO_2 was electrodeposited using an aqueous solution of manganese acetate tetrahydrate (0.1 M) with anhydrous sodium sulfate (0.1 M). In a conventional three-electrode cell setup, a LIG film (1 cm^2) was used as the working electrode, and an Ag/AgCl a and a Pt wire as the reference and counter electrode, respectively. LIG/MnO_2 electrodes were prepared at different deposition times: 1, 3, and 5 min at a potential of 0.9 V (vs Ag/AgCl). The prepared electrodes were washed and left to dry overnight under room conditions.

Electrode Characterization: The morphology of the electrodes was analyzed by scanning electron microscopy (SEM) images taken with a tabletop microscope TM3030 Plus Hitachi with an accelerating potential of 10 kV. Elemental analysis by energy dispersive spectroscopy (EDS) was also performed using the same instrument. Vibrational analyses were also conducted on the LIG and LIG/MnO_2 films using a Renishaw inViaTM Qontor confocal Raman microscope equipped with a Renishaw Centrus 2957T3, using a 50x objective lens. Measurements were conducted using a 633 nm (red) excitation laser with an exposure time of 10 s. The surface properties of the samples were investigated by X-ray photoelectron spectroscopy (XPS) using a Kratos Axis Supra spectrometer equipped with a monochromated Al Ka beam (1486.6 eV). Electrical sheet resistance (Ω sq^{-1}) measurements were taken using the Van der Pauw geometry in a Biorad HL 5500 equipment at room conditions.

Assembly and Electrochemical Evaluation of LIG/-MnO_2-Based Supercapacitors: LIG/MnO_2 electrodes were used to develop supercapacitors in a sandwich configuration. First, an electrolyte based on poly(vinyl alcohol) (PVA) and lithium chloride (LiCl) was prepared by mixing 4 g of PVA in 40 mL of distilled water at 90 °C under continuous stirring. After complete solubilization of the PVA, 8.5 mg of LiCl was added to the solution. The mixture was kept under continuous stirring and heating until it became a transparent gel. To fabricate the supercapacitors, a piece of Whatman grade 4 paper was soaked in the PVA/LiCl electrolyte and then positioned between two identical LIG/MnO_2 electrodes, acting as both a dielectric separator and as an electrolyte holder. This piece of paper was cut to dimensions slightly larger than the LIG/MnO_2 electrodes to avoid short circuits. The performance of the devices was evaluated using conventional electrochemical techniques. Cyclic voltammetry (CV) was performed in the symmetric supercapacitors using a potential window of 0 to 0.8 V and scan rates of 5 to 100 mV s^{-1}. Galvanostatic charge–discharge (GCD) measurements were also performed on the devices using a maximum charge voltage of 0.8 V. The devices were subjected to charge/discharge current densities ranging from 0.1 to 1 mA cm^{-2}. In addition, electrochemical impedance spectroscopy (EIS) analyses were performed in the frequency range of 1 MHz to 1 Hz, with an AC voltage applied at a maximum amplitude of 10 mV. The specific areal capacitance, C_A, was calculated from the CV curves using Equation (1):

$$C_A = \frac{1}{2n\Delta VA} \int I(V)\, d(V) \tag{1}$$

where ΔV stands for the applied potential window, n is the scan rate ($V\,s^{-1}$), A is the area of one electrode (cm^2), and $\int I(V)d(V)$ is the curve area enclosed by one complete CV cycle, i.e., the area within the forward and reverse scan curves. Similarly, the capacitance was also calculated from the GCD curves, according to Equation (2):

$$C_A = \frac{I}{(\Delta V/\Delta t)\, A} \tag{2}$$

In this equation, ΔV stands for the voltage variation during the discharge process; Δt is the discharge time; and I is the current density applied during the discharge process (mA cm^{-2}): The areal energy (E_A) and power (P_A) densities are important metrics to evaluate the performance of energy storage devices. These values can be calculated from GCD discharge curves using Equations (1) and (2), respectively:

$$E_A = \frac{V^2}{7200}\, C_A \tag{3}$$

$$P_A = 3600 \frac{E_A}{\Delta t} \tag{4}$$

Supporting Information

Supporting Information is available from the Wiley Online Library or from the author.

Acknowledgements

This work was supported by São Paulo Research Foundation (FAPESP), Grant #2021/14141-1, Grant #2018/02604-4 and 2022/12332-7, Programa de Pós-graduação em Ciência e Tecnologia de Materiais (POSMAT), Coordenação de Aperfeiçoamento de Pessoal de Nível Superior (Capes), and Instituto Nacional de Eletrônica Orgânica (INEO). This work was also financed by national funds from FCT – Fundação para a Ciência e a Tecnologia, I.P., in the scope of the projects LA/P/0037/2020, UIDP/50025/2020 and UIDB/50025/2020 of the Associate Laboratory Institute of Nanostructures, Nanomodelling and Nanofabrication – i3N, Individual Call to Scientific Employment Stimulus – 2nd Edition (CEECIND/00880/2018) and the project GAMBIT (2022.01493.PTDC). This work was also partially supported by the European Union's Horizon Europe research and innovation program under grant agreement number 101096021 (SUPERIOT, HORIZON-JU-SNS-2022-STREAM-B-01-03). T. Pinheiro acknowledges funding from FCT I.P. through the PhD Grant DFA/BD/8606/2020. J.C. also acknowledges the EMERGIA Junta de Andalucia program (EMC21_00174).

Conflict of Interest

The authors declare no conflict of interest.

Data Availability Statement

The data that support the findings of this study are available from the corresponding author upon reasonable request.

© 2024 The Author(s). Advanced Sustainable Systems published by Wiley-VCH GmbH

23667486, 2024, 12, Downloaded from https://advanced.onlinelibrary.wiley.com/doi/10.1002/adsu.202400254 by Universidade Estadual Paulista, Wiley Online Library on [05/11/2026]. See the Terms and Conditions (https://onlinelibrary.wiley.com/terms-and-conditions) on Wiley Online Library for rules of use; OA articles are governed by the applicable Creative Commons License

Keywords

energy storage, laser-induced-graphene, paper electronics, supercapacitor, sustainable fabrication

Received: April 12, 2024
Revised: July 15, 2024
Published online: July 24, 2024

[1] R. Lakra, R. Kumar, P. Kumar Sahoo, D. Thatoi, A. Soam, P. K. Sahoo, D. Thatoi, A. Soam, P. Kumar Sahoo, D. Thatoi, A. Soam, P. K. Sahoo, D. Thatoi, A. Soam, *Inorg. Chem. Commun.* **2021**, *133*, 108929.
[2] A. Velasco, Y. K. Ryu, A. Hamada, A. de Andrés, F. Calle, J. Martinez, *Nanomaterials* **2023**, *13*, 788.
[3] A. Imbrogno, J. Islam, C. Santillo, R. Castaldo, L. Sygellou, C. Larrigy, R. Murray, E. Vaughan, M. K. Hoque, A. J. Quinn, D. Iacopino, *ACS Appl. Electron. Mater.* **2022**, *4*, 1541.
[4] J. Coelho, R. F. Correia, S. Silvestre, T. Pinheiro, A. C. Marques, M. R. P. Correia, J. V. Pinto, E. Fortunato, R. Martins, *Microchim. Acta.* **2023**, *190*, 1.
[5] S. L. Silvestre, T. Pinheiro, A. C. Marques, J. Deuermeier, J. Coelho, R. Martins, L. Pereira, E. Fortunato, *Flex. Print. Electron.* **2022**, *7*, 035021.
[6] S. Nandy, S. Goswami, A. Marques, D. Gaspar, P. Grey, I. Cunha, D. Nunes, A. Pimentel, R. Igreja, P. Barquinha, L. Pereira, E. Fortunato, R. Martins, *Adv. Mater. Technol.* **2021**, *6*, 2000994.
[7] F. Mahmood, F. Mahmood, H. Zhang, J. Lin, C. Wan, *ACS Omega* **2020**, *5*, 14611.
[8] A. Lamberti, F. Perrucci, M. Caprioli, M. Serrapede, M. Fontana, S. Bianco, S. Ferrero, E. Tresso, *Nanotechnology* **2017**, *28*, 174002.
[9] A. Lamberti, F. Clerici, M. Fontana, L. Scaltrito, *Adv. Energy Mater.* **2016**, *6*, 1600050.
[10] T. Pinheiro, R. Correia, M. Morais, J. Coelho, E. Fortunato, M. G. F. Sales, A. C. Marques, R. Martins, *ACS Nano* **2022**, *16*, 20633.
[11] S. Parthiban, S. Saravanan, S. Hemasilviavinothini, A. Sivalingam, K. Syed, *Materials Today: Proc.* , Elsevier, Amsterdam **2023**.
[12] M. Reina, A. Scalia, G. Auxilia, M. Fontana, F. Bella, S. Ferrero, A. Lamberti, *Adv. Sustain. Syst.* **2022**, *6*, 2100228.
[13] M. F. El-Kady, M. Ihns, M. Li, J. Y. Hwang, M. F. Mousavi, L. Chaney, A. T. Lech, R. B. Kaner, *Proc. Natl. Acad. Sci. USA* **2015**, *112*, 4233.
[14] L. Lei, Z. Cao, J. Li, H. Hu, D. Ho, *ACS Appl. Energy Mater.* **2022**, *5*, 12790.
[15] X. Sun, X. Liu, X. Xing, F. Li, *J. Alloys Compd.* **2022**, *893*, 162230.
[16] G. K. Maron, M. G. Masteghin, V. Gehrke, L. S. Rodrigues, J. H. Alano, J. H. H. Rossato, V. R. Mastelaro, J. Dupont, M. T. Escote, S. R. P. Silva, N. L. V. Carreno, *Mater. Res. Bull.* **2023**, *168*, 112490.
[17] N. F. Santos, J. Rodrigues, S. O. Pereira, A. J. S. Fernandes, T. Monteiro, F. M. Costa, *Sci. Rep.* **2021**, *11*, 1.
[18] R. Ye, D. K. James, J. M. Tour, *Acc. Chem. Res.* **2018**, *51*, 1609.
[19] Y. Chyan, J. Cohen, W. Wang, C. Zhang, J. M. Tour, *ACS Appl. Nano Mater.* **2019**, *2*, 3007.
[20] Y. Chyan, R. Ye, Y. Li, S. P. Singh, C. J. Arnusch, J. M. Tour, *ACS Nano* **2018**, *12*, 2176.
[21] Z. Ismail, *Carbon Lett.* **2022**, *32*, 1227.
[22] Y. Wang, D. C. Alsmeyer, R. L. McCreery, *Chem. Mater.* **1990**, *2*, 557.
[23] A. C. Ferrari, *Solid State Commun.* **2007**, *143*, 47.
[24] A. Kaniyoor, S. Ramaprabhu, *AIP Adv.* **2012**, *2*, 32183.
[25] D. L. Costa E Silva, L. R. Pires Kassab, A. D. dos Santos, M. F. Pillis, *Mater. Res.* **2018**, *21*, e20170787.
[26] F. Mahmood, C. Zhang, Y. Xie, D. Stalla, J. Lin, C. Wan, *RSC Adv.* **2019**, *9*, 22713.
[27] A. C. Ferrari, J. C. Meyer, V. Scardaci, C. Casiraghi, M. Lazzeri, F. Mauri, S. Piscanec, D. Jiang, K. S. Novoselov, S. Roth, A. K. Geim, *Phys. Rev. Lett.* **2006**, *97*, 187401.
[28] F. J. Romero, A. Salinas-Castillo, A. Rivadeneyra, A. Albrecht, A. Godoy, D. P. Morales, N. Rodriguez, *Nanomaterials* **2018**, *8*, 517.
[29] T. Pinheiro, S. Silvestre, J. Coelho, A. C. Marques, R. Martins, M. G. F. Sales, E. Fortunato, *Adv. Mater. Interfaces* **2021**, *8*, 2101502.
[30] B. Kulyk, B. F. R. Silva, A. F. Carvalho, S. Silvestre, A. J. S. Fernandes, R. Martins, E. Fortunato, F. M. Costa, *ACS Appl. Mater. Interfaces* **2021**, *13*, 10210.
[31] H. Awasthi, U. S. Jayapiriya, H. Renuka, M. D. Wagh, A. Kothuru, A. K. Srivastava, S. Goel, *IEEE Sens. J.* **2023**, *23*, 24078.
[32] Z. Long-fei, Q. Hong-mei, X. Mei, L. Yan-zhen, H. Jian-ling, W. Zi-ya, W. Feng-ping, Z. Long-fei, Q. Hong-mei, X. Mei, L. Yan-zhen, H. Jian-ling, W. Zi-ya, W. Feng-ping, *Chin. J. Eng.* **2016**, *38*, 1300.
[33] Z. Yong, C. Cui-rong, W. Shi-wen, G. Hai-li, Y. Ji, J. Xiao-dong, L. He-wei, G. Ke-zheng, Z. Ai-qin, Z. Yong, C. Cui-rong, W. Shi-wen, G. Hai-li, Y. Ji, J. Xiao-dong, L. He-wei, G. Ke-zheng, Z. Ai-qin, *Chin. J. Eng.* **2019**, *41*, 646.
[34] N. Elgrishi, K. J. Rountree, B. D. McCarthy, E. S. Rountree, T. T. Eisenhart, J. L. Dempsey, *J. Chem. Educ.* **2018**, *95*, 197.
[35] Y. Wang, Z. Niu, J. Chen, Y. Zhai, Y. Xu, S. Luo, *Carbon N Y* **2019**, *153*, 472.
[36] Y. Li, D. X. Luong, J. Zhang, Y. R. Tarkunde, C. Kittrell, F. Sargunaraj, Y. Ji, C. J. Arnusch, J. M. Tour, *Adv. Mater.* **2017**, *29*, 1700496.
[37] C. G. Jothi Prakash, R. Prasanth, *J. Mater. Sci.* **2020**, *56*, 108.
[38] T. H. Wu, D. Hesp, V. Dhanak, C. Collins, F. Braga, L. J. Hardwick, C. C. Hu, *J. Mater. Chem. A Mater.* **2015**, *3*, 12786.
[39] C. Julien, M. Massot, R. Baddour-Hadjean, S. Franger, S. Bach, J. P. Pereira-Ramos, *Solid State Ion* **2003**, *159*, 345.
[40] Y. Dai, K. Wang, J. Zhao, J. Xie, *J. Power Sources* **2006**, *161*, 737.
[41] F. Buciuman, F. Patcas, R. Craciun, D. R. T. Zahn, *Phys. Chem. Chem. Phys.* **1999**, *1*, 185.
[42] M. Bernard, A. H. Goff, B. V. Thi, S. C. de Torresi, *J. Electrochem. Soc.* **1993**, *140*, 3065.
[43] S.-C. Pang, M. A. Anderson, T. W. Chapman, *J. Electrochem. Soc.* **2000**, *147*, 444.
[44] S. Devaraj, N. Munichandraiah, *J. Phys. Chem. C* **2008**, *112*, 4406.
[45] J. H. Jeong, J. W. Park, D. W. Lee, R. H. Baughman, S. J. Kim, *Sci. Rep.* **2019**, *9*, 1.
[46] F. Moulai, N. Cherchour, B. Messaoudi, L. Zerroual, *Ionics (Kiel)* **2017**, *23*, 453.
[47] B. Huang, X. Zhang, J. Cai, W. Liu, S. Lin, *J. Appl. Electrochem.* **2019**, *49*, 767.
[48] O. Sadak, W. Wang, J. Guan, A. K. Sundramoorthy, S. Gunasekaran, *ACS Appl. Nano Mater.* **2019**, *2*, 4386.
[49] P. Plate, C. Höhn, U. Bloeck, P. Bogdanoff, S. Fiechter, F. F. Abdi, R. van de Krol, A. C. Bronneberg, *ACS Appl. Mater. Interfaces* **2021**, *13*, 2428.
[50] D. Banerjee, H. W. Nesbitt, *Geochim. Cosmochim. Acta* **1999**, *63*, 3025.
[51] M. C. Biesinger, B. P. Payne, A. P. Grosvenor, L. W. M. Lau, A. R. Gerson, R. S. C. Smart, *Appl. Surf. Sci.* **2011**, *257*, 2717.
[52] Q. Lu, Q. Zhu, W. Guo, X. Li, *Ionics (Kiel)* **2019**, *25*, 3107.
[53] S. K. Ghosh, *ACS Omega* **2020**, *5*, 25493.
[54] X. Li, L. Yi, Q. Zhu, L. Zhao, Y. Xu, M. Liu, T. Liu, Q. Wu, *Environ. Technol.* **2021**, *42*, 81.
[55] Z. Yang, J. Lv, H. Pang, W. Yan, K. Qian, T. Guo, Z. Guo, *Sci. Rep.* **2015**, *5*, 1.
[56] M. Huang, F. Li, F. Dong, Y. X. Zhang, L. L. Zhang, *J Mater Chem A Mater* **2015**, *3*, 21380.
[57] J. E. ten Elshof, Y. Wang, *Small Methods* **2019**, *3*, 1800318.
[58] L. Cui, C. Cheng, F. Peng, Y. Yang, Y. Li, M. Jia, X. Jin, *New J. Chem.* **2019**, *43*, 14084.

© 2024 The Author(s). Advanced Sustainable Systems published by Wiley-VCH GmbH

23667486, 2024, 12, Downloaded from https://advanced.onlinelibrary.wiley.com/doi/10.1002/adsu.202400254 by Universidade Estadual Paulista, Wiley Online Library on [05/11/2026]. See the Terms and Conditions (https://onlinelibrary.wiley.com/terms-and-conditions) on Wiley Online Library for rules of use; OA articles are governed by the applicable Creative Commons License

[59] B. E. Conway, *Electrochemical Supercapacitors*, Springer Science & Business Media, Berlin, Germany **1999**.
[60] C. Zhu, X. Dong, X. Mei, M. Gao, K. Wang, D. Zhao, *J. Mater. Sci.* **2020**, *55*, 17108.
[61] C. Zhu, X. Dong, X. Mei, M. Gao, K. Wang, D. Zhao, *Appl. Surf. Sci.* **2021**, *568*, 150978.
[62] L. Li, J. Zhang, Z. Peng, Y. Li, C. Gao, Y. Ji, R. Ye, N. D. Kim, Q. Zhong, Y. Yang, H. Fei, G. Ruan, J. M. Tour, *Adv. Mater.* **2016**, *28*, 838.
[63] L. Lu, D. Zhang, Y. Xie, W. Wang, *J. Energy Storage* **2022**, *51*, 104458.
[64] C. Liu, H. Liang, D. Wu, X. Lu, Q. Wang, *Adv. Electron. Mater.* **2018**, *4*, 1800092.
[65] Z. Peng, J. Lin, R. Ye, E. L. G. Samuel, J. M. Tour, *ACS Appl. Mater. Interfaces* **2015**, *7*, 3414.
[66] P. Bhojane, *J. Energy Storage* **2022**, *45*, 103654.
[67] Z. Hu, X. Xiao, C. Chen, T. Li, L. Huang, C. Zhang, J. Su, L. Miao, J. Jiang, Y. Zhang, J. Zhou, *Nano Energy* **2015**, *11*, 226.
[68] M. R. R. Abdul-Aziz, A. Hassan, A. A. R. Abdel-Aty, M. R. Saber, R. Ghannam, B. Anis, H. Heidari, A. S. G. Khalil, *IEEE Access* **2020**, *8*, 200573.
[69] S. A. H. Moradi, N. Ghobadi, F. Zahrabi, *J. Mater. Sci.: Mater. Electron.* **2022**, *33*, 18356.
[70] P. Zaccagnini, D. di Giovanni, M. G. Gomez, S. Passerini, A. Varzi, A. Lamberti, *Electrochim. Acta* **2020**, *357*, 136838.
[71] F. Tehrani, M. Beltrán-Gastélum, K. Sheth, A. Karajic, L. Yin, R. Kumar, F. Soto, J. Kim, J. Wang, S. Barton, M. Mueller, J. Wang, *Adv. Mater. Technol.* **2019**, *4*, 1900162.
[72] J. B. Lee, J. Jang, H. Zhou, Y. Lee, J. Bin In, *Energies* **2020**, *13*, 6567.
[73] L. Lu, D. Zhang, Y. Xie, W. Wang, *J. Energy Storage* **2022**, *51*, 104458.
[74] R. Abreu, M. dos Santos Klem, T. Pinheiro, J. Vaz Pinto, N. Alves, R. Martins, E. Carlos, J. Coelho, *FlatChem* **2024**, *46*, 100672.
[75] M. Wang, J. Chen, K. Lu, Y. Ma, H. Li, J. Ye, *Electrochim. Acta* **2022**, *401*, 139490.
[76] K. Lu, Y. Ma, J. Ye, *J. Power Sources* **2022**, *535*, 231488.
[77] B. K. Ostafiychuk, I. M. Budzulyak, B. I. Rachiy, M. M. Kuzyshyn, L. O. Shyyko, *Nanosci. Nanotechnol. Res.* **2013**, *1*, 17.
[78] J.-H. Jeong, J. W. Park, D. W. Lee, R. H. Baughman, S. J. Kim, *Sci. Rep.* **2019**, *9*, 11271.

© 2024 The Author(s). Advanced Sustainable Systems published by Wiley-VCH GmbH

23667486, 2024, 12, Downloaded from https://advanced.onlinelibrary.wiley.com/doi/10.1002/adsu.202400254 by Universidade Estadual Paulista, Wiley Online Library on [05/11/2026]. See the Terms and Conditions (https://onlinelibrary.wiley.com/terms-and-conditions) on Wiley Online Library for rules of use; OA articles are governed by the applicable Creative Commons License